Title

Correction of B0-Distortions in Echo-Planar-Imaging–Based Perfusion-Weighted MRI

Journal

Journal of Magnetic Resonance Imaging, 39(3)

ISSN

1053-1807

Authors

Vardal, Jonas
Salo, Raimo A
Larsson, Christopher
et al.

Publication Date

2014-03-01

DOI

10.1002/jmri.24213

Peer reviewed

Technical Note

Correction of B0-Distortions in Echo-Planar-Imaging–Based Perfusion-Weighted MRI

Jonas Vardal,[1,2]* Raimo A. Salo, MS,[1] Christopher Larsson,[1,2] Anders M. Dale, PhD,[5,6,7] Dominic Holland, PhD,[5,6] Inge Rasmus Groote, PhD,[3] and Atle Bjørnerud, PhD[1,4]

Purpose: To evaluate and quantify a scheme for correcting susceptibility artifacts in spin-echo echo-planar-imaging–based dynamic susceptibility contrast (DSC) perfusion MRI of high-grade gliomas at 3 Tesla.

Materials and Methods: Sixteen patients with a total of 78 scans were studied. DSC-MRI images were corrected using a displacement map generated from opposite phase-encoding polarity images. Two methods were used for quantification in the correction: (i) linear regression of pixel-by-pixel comparisons, performed both globally and relative to the anterior and posterior commissure plane (AC-PC plane), of T2-weighted images with both corrected and uncorrected raw DSC images; and (ii) counting significant (>2.0) normalized cerebral blood volume (nCBV) pixels from perfusion maps in the tumor region of interest.

Results: Sixty-four of 78 datasets showed significant differences in the coefficient of correlation (r^2) values. The difference between corrected and uncorrected r^2 values was positive in all but one patient. Correction of B0-distortion significantly improved r^2 in slices around the AC-PC plane. In 62% of the datasets, we observed an increased number of significant pixels in the corrected nCBV maps; 36% showed more significant pixels in uncorrected nCBV maps; 1% showed no difference.

Conclusion: Distortion correction of DSC-MRI may provide improved accuracy compared with uncorrected data, especially for tumors located below the corpus callosum and near the frontal sinuses.

Key Words: EPI; DSC-MRI; correction; distortion; artifacts; glioma
J. Magn. Reson. Imaging 2014;39:722–728.

CEREBRAL PERFUSION IMAGING provides unique insight into brain pathophysiology and is increasingly used in the diagnosis and therapeutic follow-up of brain diseases such as ischemia, cancer, and epilepsy (1–3). Brain hemodynamics can be assessed using various radiation-based modalities, including positron emission tomography (PET), single photon emission computed tomography (SPECT), and X-ray computed tomography (CT), whereas MRI provides a nonionizing alternative (4). Contrast-enhanced perfusion-weighted MRI (pMRI) is most commonly performed using dynamic susceptibility contrast (DSC) imaging, which relies on an ultra-fast spin-echo (SE) or gradient-echo (GRE) echo-planar-imaging (EPI) sequence to track a bolus of gadolinium-containing contrast agent (CA) in an acquisition with a temporal resolution of the order of 1–2 s. Subsequent modeling of temporal signal changes is then used to estimate several clinically relevant hemodynamic parameters, such as cerebral blood volume (CBV), cerebral blood flow (CBF), and mean transit time (MTT) (5).

It is well known that EPI suffers from severe spatial- and intensity distortions due to B0-field inhomogeneity induced by magnetic susceptibility variations (6). Distortions typically occur around interfaces between tissues with different magnetization, for example over air–tissue boundaries (e.g., near the sinuses) (7), and around metal implants and drill debris from surgical procedures (8). Distortion in EPI is most pronounced in the phase-encoding (PE) direction because of the long time between sampling points (low bandwidth) relative to the readout direction, during which there can be substantial change in phase accumulation due to field inhomogeneities (9). An increase in static magnetic field strength, B0, will proportionally increase distortions because the magnetization variation is

[1]Oslo University Hospital, Rikshospitalet, The Intervention Centre, Oslo, Norway
[2]University of Oslo, Faculty of Medicine, Oslo, Norway
[3]University of Oslo, Institute of Psychology, Oslo, Norway
[4]University of Oslo, Faculty of Physics, Oslo, Norway
[5]Multimodal Imaging Laboratory, The University of California, San Diego, California, USA
[6]Department of Neurosciences, The University of California, San Diego, California, USA
[7]Department of Radiology, The University of California, San Diego, California, USA
*Address reprint requests to: J.V., Oslo universitetssykehus HF, Rikshospitalet, Postboks 4950 Nydalen, 0424 Oslo, Norway. E-mail: jonas.vardal@medisin.uio.no
Received November 21, 2012; Accepted April 15, 2013
DOI 10.1002/jmri.24213
View this article online at wileyonlinelibrary.com.

directly proportional to B0 (8), and pixel displacements of the order of centimeters may be expected at 3 Tesla (T) in areas with substantial susceptibility variations (10). The presence of such large distortions in EPI images complicates spatial correlation with corresponding undistorted structural scans, severely limiting the accuracy and usefulness of EPI-based information for stereotactic biopsy and surgery (11). Although DSC data suffers primarily from these large geometric distortions, it should be noted that additional time-dependent artifacts may occur, manifested as geometric displacement of vessels during CA bolus passage (12).

Numerous approaches have been suggested to reduce distortion in EPI images. By improving the sequence, distortions can be reduced primarily by increasing the pixel bandwidth in the PE direction. Ultimately, this approach is limited by the available gradient strength and requirements of maintaining both high spatial resolution and signal-to-noise ratio (SNR). Several correction procedures based on retrospective postprocessing have, therefore, been proposed, to reduce distortions beyond what is achievable by sequence optimization alone. The most common of these is a method in which the field inhomogeneity is estimated from the phase difference between a pair of GRE images acquired using different echo times (13). Performing phase map-based unwarping of EPI images requires minutes of additional data acquisition, thus increasing the chances of intra-scan subject motion, which can lead to large errors in the resulting field map.

An alternative approach to reducing EPI image distortions is the reversed gradient method (14) using an acquisition scheme in which an additional EPI image volume, identical to the first dynamic precontrast volume, except for the reversed polarity of the PE gradient, is acquired. This requires a maximum of 10 extra s of acquisition time. The reversed gradient polarity method is based on the following fact: If *k*-space is traversed in the opposite direction along the PE axis, then the distortions will be precisely reversed. The undistorted, anatomically correct image is then midway between the two oppositely distorted images and can be estimated directly from the EPI magnitude images of opposite PE polarity. This method is attractive in a clinical setting because of the much-reduced overhead: less scan time is needed because only a single additional EPI-volume is required and the acquisition of EPI with reversed PE polarity can be readily obtained on most modern scanners with no need for special sequence development. Additional advantages include reduced patient scan-time burden and institutional MRI usage.

The reversed PE gradient method has previously proved effective for correcting geometric distortions in SE-EPI data in general but the method has thus far mainly been applied to diffusion weighted- and tensor imaging (DWI/DTI) (15,16) and functional MRI (fMRI) (17). Also, there has been little focus on testing the utility of such correction schemes in specific clinical applications. To this end, the main purpose of the present work was to test one implementation of the reversed gradient method for DSC-based perfusion imaging of glioma patients, a relevant and important patient population and an application where EPI-based imaging is very commonly performed.

DSC acquisitions differ from other EPI applications in that they exhibit a substantial dynamic signal variation (due to the contrast agent bolus passage), and it is therefore particularly important to verify that any correction scheme applied to the raw EPI-data does not degrade the quality of the derived perfusion dependent parametric images.

This study investigates the feasibility of using this correction approach to generate higher quality EPI-based pMRI data. Improved spatial correspondence to undistorted image sets, achieved with very little imaging- and minor postprocessing time requirements, would potentially increase the clinical utility of DSC in procedures such as functional neurosurgery, stereotactic biopsy, and radiation planning.

METHODS

Patient Selection

The study was approved by the Regional Medical Ethics Committee and patients were enrolled only if informed consent was obtained. A total of 16 patients (11 men; 5 women), aged 33–68, were included: 13 had glioblastoma multiforme, two had anaplastic astrocytoma and one had anaplastic oligodendroglioma, all biopsy- or post-resection-confirmed. Fourteen patients received radiotherapy and concomitant temozolomide therapy; two received radiotherapy alone. Data were acquired before the first dose of radiotherapy, every other week for the following 8 weeks, and again every 3 months after radiotherapy was completed, resulting in a total of 78 data sets included in the study.

MRI

Imaging was performed at 3T (Philips Achieva, Philips Medical Systems, Best, Holland), using an eight-channel SENSE head coil (Invivo, FL).

Structural Scans

A structural imaging protocol for direct geometric comparisons and spatial registration procedures included the following: a sagittal whole-brain three-dimensional (3D) fluid-attenuated inversion-recovery (FLAIR) sequence, a 2D axial T2-weighted (T2-w) turbo SE sequence, and a sagittal whole brain 3D T1-weighted (T1-w) spoiled GRE sequence with and without gadobutrol (Gadovist™, Bayer Schering Pharma AG, Berlin, Germany) contrast enhancement. The CA-enhanced T1-weighted series was acquired after the pMRI series to avoid excessive contrast enhancement. The following sequence parameters were used (repetition time/echo time/inversion time [TR/TE/TI]): FLAIR (8000 ms/417 ms/2400 ms), field of view (FOV) 240 × 240 mm=, slice thickness = 1.2 mm, SENSE factor = 2; T2-w (3000 ms/80 ms), FOV 230 × 230 mm^2, slice thickness = 2.5 mm; T1-w (5.0 ms/

2.2 ms), FOV 256 × 256 mm^2, slice thickness = 1.0 mm, SENSE factor = 2.

DSC

DSC images were acquired using a 2D single-shot SE-EPI with the following imaging parameters: TR/TE 1341 ms/70 ms, FOV 240 × 240 mm^2, voxel size 2 × 2 × 4 mm^3, 13 slices, SENSE factor = 2 in the PE direction, pixel bandwidth 2438 Hz (frequency encoding direction) and 28.3 Hz (PE direction), 80 time points. After five time points, 0.1 mmol/kg of gadobutrol was injected at a rate of 5 mL/s using a power injector (MEDRAD, Spectris Solaris® EP MR Injection System), immediately followed by a 20-mL flushing bolus of saline.

DSC Image Unwarping

Distortion correction was performed by acquiring two precontrast SE-EPI image volumes with geometry and image parameters identical to those of the DSC images but with opposing PE polarity (Anterior–Posterior or Posterior–Anterior). Displacement maps were generated by identifying corresponding voxels in the oppositely phase-encoded (oppositely distorted) baseline (precontrast) SE-EPI images. This was done by first heavily smoothing both images and then minimizing a smooth merit function that depends on the voxel-wise difference in intensities between these images. High smoothing leads to a high degree of similarity between the images; as a result, the merit function can be approximated by expanding it in a Taylor series to second order. This approximate form of the merit function can expeditiously be minimized by standard numerical techniques; generically, the minimization is a second-order Newton's method. The result is a displacement field that matches the smoothed images, taking into account intensity variation that arises from spin bunching and distension. This displacement field is then taken as a starting point for matching images with less smoothing, and the whole process iterated until there is no smoothing (18). The resulting displacement maps were then applied to the DSC images, creating geometrically and intensity corrected dynamic image series. Figure 1 shows a sample axial slice of two SE-EPI images with opposite polarity and the resulting corrected image.

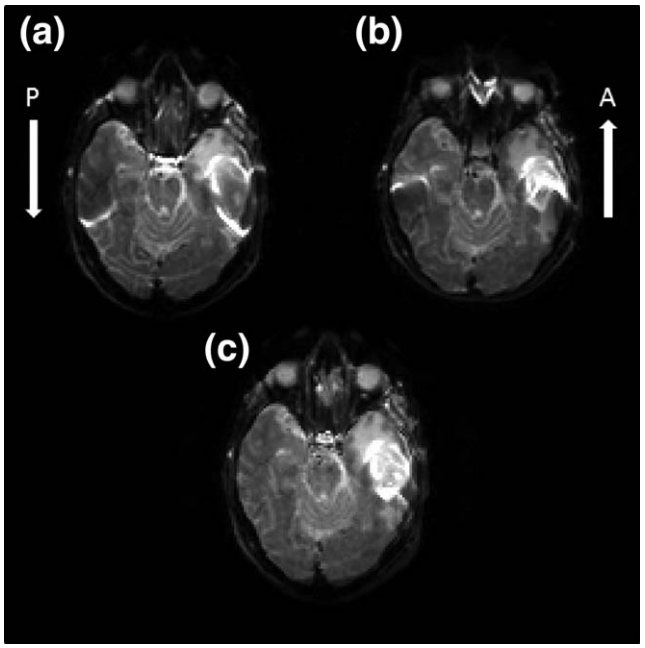

Figure 1. Example of geometric distortion in two SE-EPI images (**a**,**b**) with opposite phase encoding gradient (P = posterior; A = anterior) in a postsurgical tumor, compared with a corrected DSC-MRI image (**c**).

Analysis

Structural Correlation

Quantifying the degree of anatomical fit in the corrected and uncorrected DSC data was achieved by comparing DSC images with and without EPI-correction to undistorted T2-w images. Because SE-EPI-images are strongly T2-w, a linear correlation between the pixel-wise signal intensity in the precontrast DSC images and the T2-w images would be expected following co-registration and spatial smoothing. Furthermore, the linear correlation would be expected to be highest in the DSC images, with the least amount of geometric distortion relative to the (assumed) undistorted T2-w images. The first (precontrast) time-point in the DSC images was used for the correlation analysis. The opposite PE polarity images were resampled to fit the matrix size of the T2-w images. The T2-w and DSC image sets were smoothed using a 5.0-mm full-width at half-maximum (FWHM) Gaussian kernel to reduce noise. Using such a large FWHM ensures that the differences in correlation represent a definite effect. To validate this, a sample of four datasets from four different patients was selected to compare the effect of using a reduced kernel of 2.0 mm with the 5.0 mm kernel. The resulting DSC image sets were spatially rigid-body co-registered to the structural image sets (FLAIR, T1, and T2) using normalized mutual information (19). Binary brain masks were obtained by skull-stripping the FLAIR image series using the brain extraction tool (20) and used to extract brain-only pixels from both the DSC images and the T2-w images. All further analysis was performed on pixels included in this brain mask. Pixel intensities were extracted for each position in the structural and dynamic series in a slice-wise manner, enabling correlation analysis on individual slices as well as globally. A pairwise two-tailed t-test with alpha level 0.05 was performed on the coefficient of correlation (r^2) values obtained from the linear regression from the individual scans.

To clarify the difference between correlation values obtained from corrected and uncorrected images, a slice-wise subtraction of correlation values (corrected – uncorrected) was performed and averaged across slices for each patient.

Image co-registration and image analysis was performed using the nordicICE software tool (NordicNeuroLab AS, Bergen, Norway) and EPI unwarping was performed using Epic (*EPI* correction), software (18).

Linear Relation to Anterior and Posterior Commissure Plane

Being able to determine where the corrections have the strongest effect relative to anatomical location in the brain may demonstrate in which situations the unwarping should be used. To accomplish this, a linear slice-wise comparison was made where each slice of the first dynamic DSC volume was defined in terms of its distance from the anterior and posterior commissure plane (AC-PC plane), which was set as a baseline. Slices superior to the AC-PC plane were then defined as having positive offsets, and slices inferior as negative. Some discrepancy was noted in the angular orientation between the dynamic series and the structural images relative to the AC-PC plane: a couple of degrees in each direction. Because of this variation, some slices defined as being in the AC-PC plane did not contain both. In cases where the two were in adjacent slices, the AC slice was used. If there was a slice between the AC and the PC slices, the middle one was used. Using this approach, a plot of linear correlation coefficient versus position from the AC-PC plane was obtained for each scan and the results averaged for the corrected and uncorrected data sets and restricted to the middle area where there were more than 20 geometrically overlapping datasets for averaging. This was done to ensure robustness of the comparisons.

Normalized CBV Region-of-Interest Analysis

To evaluate the corrected data in a clinical setting, a comparison of a frequently used parameter, CBV, derived from the corrected and uncorrected DSC images was performed. Relative CBV maps were automatically normalized to unaffected white matter (5). The resulting normalized CBV (nCBV) maps were coregistered to binary tumor masks generated from the structural datasets. Regions of interest (ROIs) were then extracted from the masks based on nCBV thresholds of 2.0, a typical cutoff value for active high-grade tumors (21). Information extracted from the region of interest (ROI) analysis included the total number of pixels above the nCBV cutoff, the total number of tumor pixels, the mean and the standard deviation of nCBV values. This was done to ensure validity in the corrected data.

RESULTS

Table 1 summarizes tumor location in the individual patients.

Table 1
Summary of Tumor Location in Individual Patients

Patient no.	Main localization
1, 2, 4, 6, 8, 9, 10	Temporal lobe
13, 14	Parietal lobe
3, 5, 11, 15, 16	Frontal lobe
7	Corpus callosum
12	Occipital lobe

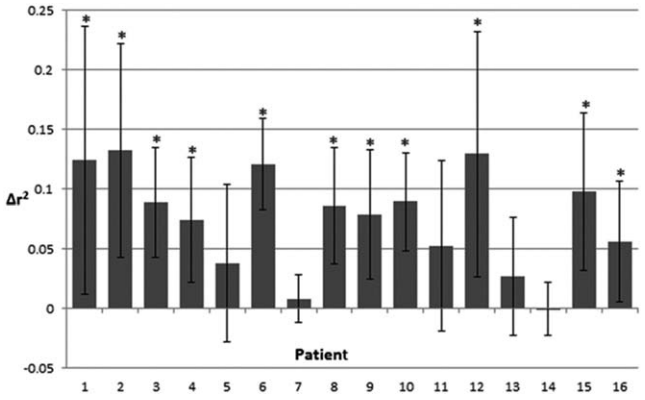

Figure 2. Mean difference in corrected and uncorrected r^2-mean values: $\Delta r^2 = r^2$ (corrected) - r^2 (uncorrected). Error bars show the 95% confidence interval across all examinations in each patient. Statistically significant Δr^2 values are indicated by asterisks. A positive Δr^2 suggests a better DSC-MRI correlation with structural scans *after* correction.

Structural Correlations

In 64 of 78 (82%) datasets, there were significant differences between the linear correlation coefficients, obtained with respect to the T2-w images, for the corrected- and uncorrected DSC images. Figure 2 shows the results for each patient of cumulative subtraction of correlation coefficients for all slices and all examinations obtained with- and without correction. In all patients except one, the correlation to T2-w images was higher after correction of the DSC images, and in 11 patients the difference was significantly different from zero ($\alpha = 0.05$). Using a 2.0-mm smoothing, instead of 5.0 mm, produced the same results for the four individual cases, except that the effects were stronger, i.e., significant *P* values were lowered and nonsignificant values were increased.

Linear Relation to AC-PC Plane

Figure 3 shows the slice position-dependent (relative to the AC-PC plane) correlation between T2-w images and DSC images for the corrected and uncorrected

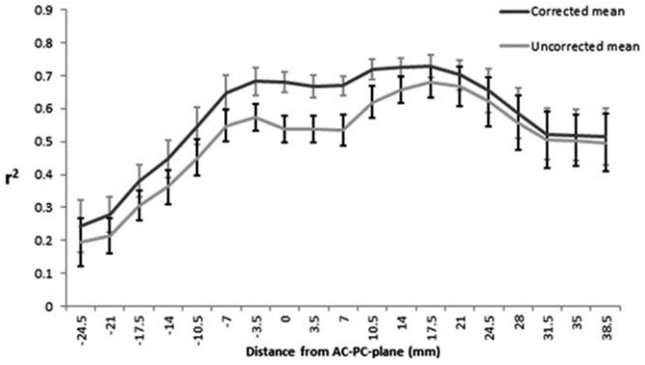

Figure 3. Mean linear correlation coefficient, r^2, between DSC-MRI and T2-w as function of slice position relative to AC-PC plane for corrected and uncorrected scans. Bars for 95% confidence interval show a significant difference between corrected and uncorrected images for the interval (−3.5–10.5 mm) around the AC-PC plane.

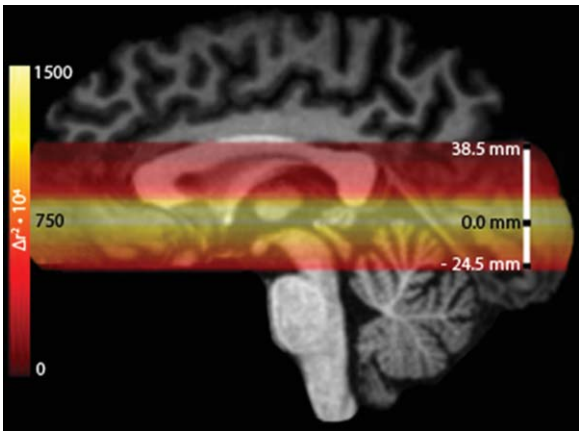

Figure 4. Visual representation of difference between corrected and uncorrected mean values related to position. Each slice was corrected independently. Color scale represents scaled Δr^2 values ($\Delta r^2 \cdot 10^4$) from Figure 3.

scans. Similar position dependence was observed for both corrected and uncorrected series, but with a higher correlation to structural data at all locations for the corrected DSC images. Figure 4 shows a graphical representation of the same results with upscaled Δr^2 values ranging from 0 to 1500 and an indication of distance from the AC-PC plane.

ROI Analysis

Tumor ROI analysis of normalized threshold values >2.0 in the nCBV-maps showed an increased number of significant pixels in the corrected image set. Analysis of a total of 78 datasets revealed 49 sets with a higher pixel-count in the corrected nCBV-maps, 28 with a higher count in uncorrected images, and one with no difference. The average (min–max) ratio of the number of nCBV values above the cutoff in the corrected data versus uncorrected data was 1.11 (0.43–

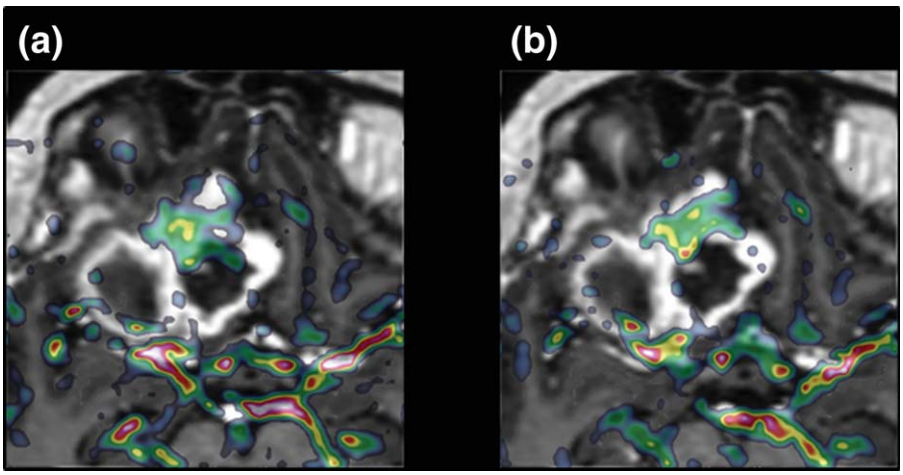

Figure 5. Example of nCBV-map (with threshold at nCBV > 2) overlaid on T1-w contrast enhanced image. The uncorrected map **(a)** shows a larger proportion of high nCBV pixels outside the contrast enhanced area; whereas the corrected map **(b)** are in better agreement with the contrast enhanced borders.

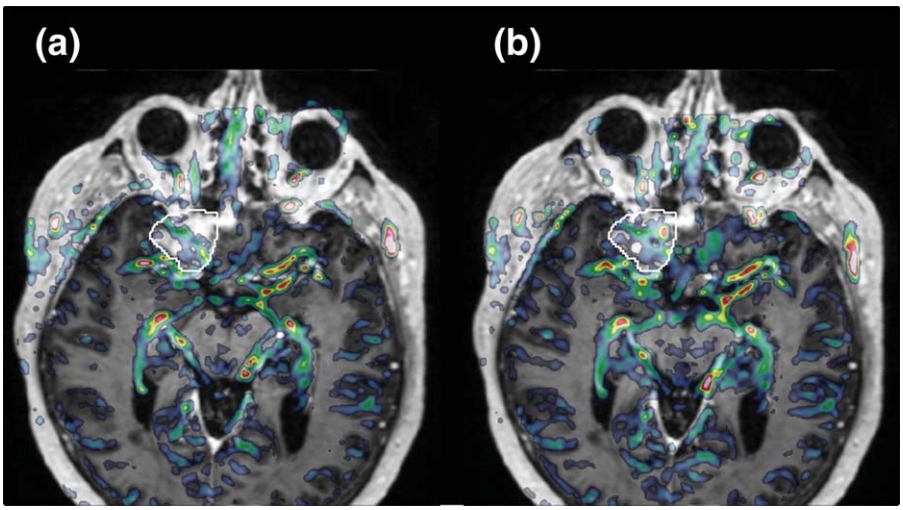

Figure 6. Additional example of uncorrected **(a)** and corrected **(b)** nCBV-maps overlaid on T1-w contrast enhanced image. Tumor contrast enhancement is highlighted with a white tumor ROI. Improvements include increased pixel-coverage of the tumor area, tumor hotspot appearing in the upper right corner of the ROI and improved overlap of nCBV over the MCA-contrast enhancement.

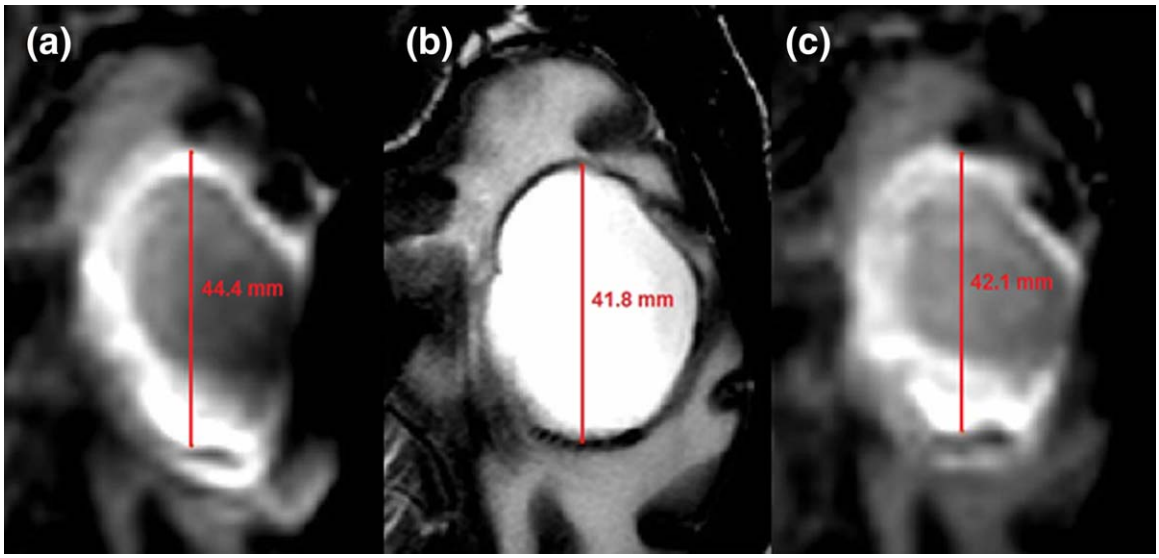

Figure 7. Measured distance of maximum diameter of tumor hyperintensity in an uncorrected (a) and corrected (c) DSC-MRI image, compared with tumor extension in T2-w (b) image. [Color figure can be viewed in the online issue, which is available at wileyonlinelibrary.com.]

2.54) ($P = 0.032$). Figure 5 and 6 shows a sample case of the improved correlation between the elevated nCBV areas derived from the DSC images and the structurally defined tumor ROI after correction.

A sample of the structural changes resulting from the correction method is shown in Figure 7. The largest diameter of the outer border of the hyper-intense region obtained from baseline SE-EPI images agrees better with the T2-w structural scan after correction.

DISCUSSION

This work addresses the potential utility of obtaining geometrically improved EPI-based DSC images using a correction algorithm based on the reversed gradient method. The reverse gradient method has previously been shown to be effective when applied to DTI (16) and fMRI data (17), but this is the first study to show its application in DSC. Our results showing improved spatial correlation to structural scans suggests that the EPI distortion correction method presented here reduces geometric distortions in DSC examinations.

Regardless of whether EPI correction was applied, the spatial correlation between the EPI- and T2-w images was found to be highly position dependent, with markedly reduced correlation in areas with increasing distance from the AC-PC plane. The improvement in correlation to structural scans offered by the EPI correction was, however, found to be greatest in a region approximately 15 mm on each side of the AC-PC plane, which suggests that the method more efficiently reduced moderate distortions compared with the severe distortions occurring in the most inferior regions.

The spatial EPI correction was also found to provide nCBV maps with larger overall number of pixels, within the structurally defined tumor ROIs, showing elevated nCBV, thus providing a more clinically relevant assessment of the applied correction scheme. This finding is, however, difficult to fully assess as there is no gold standard in pMRI.

DSC differs from other EPI-applications in terms of a temporal variation in intra- and extravascular magnetization during the CA bolus passage. This may induce additional artifacts and these are not corrected for using the presented B0-correction method. However, these are local artifacts occurring near vessels and, thus, will mainly introduce errors in determination of arterial input function (AIF) (22) and are, therefore, not expected to significantly influence the quality of AIF independent nCBV maps. Temporal properties of DSC imaging might also induce slight patient motion. This motion can be corrected for by registering later images to the initial image; provided the extent of motion is small relative to the extent of the susceptibility-induced distortions. With this assumption, the distortions can be regarded as time-independent so that the correction scheme where only the distortion from the first dynamic series is considered would remain valid.

There are limitations to this study. First, the analysis was performed in patients after surgery. Consequently, in some of the patients, surgical clips and/or debris from drilling during surgery caused significant susceptibility distortions in EPI-images in addition to those created by anatomical features. These artifacts were not significantly diminished by the correction algorithm (data not shown) but they did lead to a general reduction in the structural correlation of the EPI data relative to what likely would have been observed in preoperative patients. Furthermore, the patient group had reduced tumor volume relative to preoperative patients due to tumor debulking, making analysis of areas of elevated nCBV less robust than it might have been in preoperative high-grade glioma (HGG) patients.

Second, a comparison between different correction methods was not performed. Such a comparison would have required additional correction scans and algorithms not available in the present study.

Third, an independent or direct assessment of anatomical distortions in the EPI scans could not be performed and the effect of the correction was determined only geometrically in terms of a linear pixel-wise correlation to structural T2-w scans. The structural scans were further assumed to be minimally distorted and to exhibit a contrast weighting with a generally high correlation to the baseline DSC images. In the absence of an absolute gold standard against which the EPI scans can be assessed, both of these assumptions seem reasonable.

Finally, in the present study an SE-EPI sequence was applied for DSC imaging. For brain tumor assessment, GRE-EPI sequences are still more commonly used due to a larger CA dose-response and generally better SNR. However, both SE- and GRE-EPI sequences have been shown to provide relative CBV values in tumor hotspots that correlate with tumor grade (23). Furthermore, because we specifically investigated patients with confirmed HGGs following surgery, the use of GRE-EPI at 3T was generally found to induce unacceptable signal loss, in most cases extending into the tumor ROI due to surgical clips and drill debris from the surgical procedure. The amount of signal loss is considerably reduced in SE-EPI due to the application of 180 degree refocusing pulses, which significantly reduces intra-voxel dephasing (18) compared with GRE-EPI, thus favoring use of this EPI sequence type in postoperative HGG patients. The opposite PE polarity correction method might also have a use in GRE-EPI, using SE-EPI-based correction scans (18). This approach warrants further investigation in preoperative patient cohorts.

Despite the limitations of the present study, our results clearly indicate that the reduced distortion obtained in the B0-corrected EPI-based pMRI image series could be of major clinical importance, including other patient populations. Imaging-based navigational procedures such as presurgical biopsies, stereotactic treatment, and functional neurosurgery all gain from improved imaging precision and image co-registration (4,8,24,25); the most pronounced gains from this technique would be expected in regions of high distortion, e.g., in dealing with lesions close to air sinuses.

In conclusion distortion correction of DSC data using two SE-EPI prescans with opposite PE polarity and a correction algorithm is feasible and may provide improved accuracy relative to uncorrected data. In particular, the higher accuracy afforded would potentially reduce sampling errors during biopsy, improve surgical planning, and better anatomical correlation of observed functional changes derived from longitudinal DSC therapeutic follow-up. The methods should be considered especially in patients with tumors located below the corpus callosum or in regions around the frontal sinuses, where geometric distortions in EPI scans are most severe.

ACKNOWLEDGMENTS

We thank Knut Lote MD, PhD and Petter Brandal MD, PhD for patient recruitment.

REFERENCES

1. Law M. Advanced imaging techniques in brain tumors. Cancer Imaging 2009;9(Spec No A):S4–S9.
2. Yoo AJ, Pulli B, Gonzalez RG. Imaging-based treatment selection for intravenous and intra-arterial stroke therapies: a comprehensive review. Expert Rev Cardiovasc Ther 2011;9:857–876.
3. Lai V, Mak HK, Yung AW, Ho WY, Hung KN. Neuroimaging techniques in epilepsy. Hong Kong Med J 2010;16:292–298.
4. Wintermark M, Sesay M, Barbier E, et al. Comparative overview of brain perfusion imaging techniques. J Neuroradiol 2005;32: 294–314.
5. Bjornerud A, Emblem KE. A fully automated method for quantitative cerebral hemodynamic analysis using DSC-MRI. J Cereb Blood Flow Metab 2010;30:1066–1078.
6. Haacke EM, Brown RW. TMRVR. Magnetic resonance imaging. Physical principles and sequence design. New York: Wiley-Liss; 1999.
7. Hutton C, Bork A, Josephs O, Deichmann R, Ashburner J, Turner R. Image distortion correction in fMRI: A quantitative evaluation. Neuroimage 2002;16:217–240.
8. Schenck JF. The role of magnetic susceptibility in magnetic resonance imaging: MRI magnetic compatibility of the first and second kinds. Med Phys 1996;23:815–850.
9. Mansfield P. Multi-planar image-formation using NMR spin echoes. J Phys C Solid State Phys 1977;10:L55–L58.
10. Bowtell R, Mansfield P, Coxon RJ, Harvey PR, Glover PM. High-resolution echo-planar imaging at 3.0 T. Magn Reson Mater Phys Biol Med 1994;241–245.
11. Knopp EA, Cha S, Johnson G, et al. Glial neoplasms: dynamic contrast-enhanced T2*-weighted MR imaging. Radiology 1999;211:791–798.
12. Chang CI, Du Y, Wang J, Guo SM, Thouin PD. Survey and comparative analysis of entropy and relative entropy thresholding techniques. IEEE Proc Vision Image Signal Processing 2006;153: 837–850.
13. Jezzard P, Balaban RS. Correction for geometric distortion in echo-planar images from B-0 field variations. Magn Reson M 1995;34:65–73.
14. Chang H, Fitzpatrick JM. A technique for accurate magnetic-resonance-imaging in the presence of field inhomogeneities. IEEE Trans Med Imaging 1992;11:319–329.
15. Morgan PS, Moody AR, Allder SJ, Bowtell RW. Correction of distortion in ADC maps using the reversed gradient method. Proc Int Soc Magn Res Med 2000;8:800.
16. Ruthotto L. Diffeomorphic susceptibility artifact correction of diffusion-weighted magnetic resonance images. Phys Med Biol 2012;57:5715.
17. Embleton KV, Haroon HA, Morris DM, Ralph MA, Parker GJ. Distortion correction for diffusion-weighted MRI tractography and fMRI in the temporal lobes. Hum Brain Mapp 2010;31:1570–1587.
18. Holland D, Kuperman JM, Dale AM. Efficient correction of inhomogeneous static magnetic field-induced distortion in Echo Planar Imaging. Neuroimage 2010;50:175–183.
19. Studholme C, Hill DLG, Hawkes DJ. An overlap invariant entropy measure of 3D medical image alignment. Pattern Recognition 1999;32:71–86.
20. Smith SM. Fast robust automated brain extraction. Hum Brain Mapp 2002;17:143–155.
21. Law M, Yang S, Wang H, et al. Glioma grading: sensitivity, specificity, and predictive values of perfusion MR imaging and proton MR spectroscopic imaging compared with conventional MR imaging. AJNR Am J Neuroradiol 2003;24:1989–1998.
22. Duhamel G, Schlaug G, Alsop DC. Measurement of arterial input functions for dynamic susceptibility contrast magnetic resonance imaging using echoplanar images: comparison of physical simulations with in vivo results. Magn Reson Med 2006;55:514–523.
23. Schmainda KM, Rand SD, Joseph AM, et al. Characterization of a first-pass gradient-echo spin-echo method to predict brain tumor grade and angiogenesis. AJNR Am J Neuroradiol 2004;25:1524–1532.
24. Hunsche S, Sauner D, Treuer H, et al. Optimized distortion correction of epi-based statistical parametrical maps for stereotactic neurosurgery. Magn Reson Imaging 2004;22:163–170.
25. Novotny J Jr, Vymazal J, Novotny J, et al. Does new magnetic resonance imaging technology provide better geometrical accuracy during stereotactic imaging? J Neurosurg 2005;102(Suppl): 8–13.